Send Orders of Reprints at reprints@benthamscience.net

The Open Spectroscopy Journal, 2013, *7*, 1-8

Open Access

A Computational/Spectroscopic Study of a Newly Derived General Unified Theory of Spectral Line Shapes to Measure HWHM's for an Ar-perturber/K-radiator system, Using Two $7s \leftarrow 4p$ Transitions, as Applied to the Line Core

W. C. Kreye*

Research and Instructional Computer Center and Chemistry Department, Wright State University, Dayton, Ohio, 45435, USA

Abstract: In a recent publication, a new unified theory of spectral line shapes was derived, which allowed for the variation of the electric dipole moment with perturber positions. The present author put the $g(s)$ term derived from the theory into a computable form, and constructed spectral line shapes from which line-core HWHM's ($w's$) were measured. These w's were compared with experimental Fabry-Perot-interferometric results. Typically, for ΔV_2 and T=1000 K, the percent difference between $w_{exptl.}$ and $w_{compt.}$ is $\approx$ 22%. $log(w) - vs - log(P)$ and curve is computed and compared with those from non-impact-approximation-theory computations. Two temperatures were studied at T=400 and 1000 K in the Ar-perturber/K-radiator system; and two pseudo-potential differences were used: $\Delta V_1 = 7s^2S_{1/2} -, 4p^2P_{3/2,3/2}$ and $\Delta V_2 = 7s^2S_{1/2} - 4p^2P_{3/2,1/2}$. They were used to evaluate their comparative effects on w. E.g., ΔV_1 with a deep well exhibited a larger w than that of ΔV_2 with a shallow well.

Keywords: Quantum-mechanical, Semi-classical, Unified-theory, Spectral-line-shapes, Non-impact-approximation, K/Ar-system.

1. INTRODUCTION

In the continual development of spectral line-shape theory, one of the most important outputs of a theory is the derivation of the $g(s)$ term, defined in the Discussions subsection 6.3, because from it the line shape can be computed and the HWHM(w) can be measured and tested experimentally with spectrophotometric or interferometric techniques. Typical derivations of the $g(s)$ term are as follows: Baranger [1] derived two quantum-mechanical (QM) $g(s)$ terms, one Eq.(31)[1] for the impact approximation and one Eq.(29)[1] for the non-impact approximation; Allard and Kielkopf [2] derived two semi-classical (SC) $g(s)$ terms, two Eqs.(56,57)[2] for the impact approximation and one Eq.(55)[2] for the non-impact approximation; Szudy and Baylis [3] presented a $g(s)$ term Eq.(2.15) [3] for their unified theory; very recently, Allard *et al*. [4] published a comprehensive derivation of the $g(s)$ term Eq. (121) [4] for their unified theory of line shapes, in which the electric dipole moment varies with the position of the perturbers (see Theory Section for details of the theory). An example of the application of this unified theory is by Allard *et al*. [5] who studied the $He(3^3S) - He(2^3P)$ line.

Kreye and Kreye/Kielkopf [6-9] have used the $g(s)$ terms to compute spectral-line shapes for the line core; and from them have measured the w's and the shifts d's of the 5802 Å line for the Ar-perturber/K-radiator system at temperatures (T's) equal to 400, 800 and 1000 K. They computed and discussed $log(w) - vs - log(P)$ and $log(w) - vs - log(n)$ curves for two pseudo-potential differences, ΔV_0 = *plane wave* $- 4p^2P_{3/2,1/2}$, and $\Delta V_1 = 7s^2S_{1/2} - 4p^2P_{3/2,3/2}$. P and n are the perturber pressure and density, respectively.

In the present paper, Kreye extends the previous studies [6-9] as follows:(1) the g(s) term from the newly derived unified theory of spectral line shapes Eq.(121)[4] is put into a computable form and the w's are measured from the computed line shapes for the line core;(2) a computed non-impact-approximation $log(w) - vs - log(P)$ curve is compared

*Address correspondence to this author at the Research and Instructional Computer Center and Chemistry Department, Wright State University, Dayton, Ohio, 45435, USA; E-mail warren.kreye@wright.edu

1874-3838/13

with an earlier impact-approximation curve in [8];(3) a third pseudo-potential difference is introduced, $\Delta V_2 = 7s^2S_{1/2} - 4p^2P_{3/2,1/2}$; (4) $log(w) - vs - log(P)$ curves for the unified theory are studied at T=400 and 1000 K and compared with those from non-impact-approximation theory; (5) a question had been brought up in the previous paper [9], which shows in Fig. (**2**) [9] a slope discontinuity in the $log(w) - vs - log(P)$ curve between the impact-approximation and non-impact-approximation regions. The question was, is there any alternative method for plotting $log(w) - vs - log(P)$ curves which avoids the slope discontinuity? This paper shows that there is an alternate method for plotting $log(w) - vs - log(P)$ that avoids these slope discontinuities, as demonstrated in Fig. (**3**) and in Conclusions 5.1.

2. THEORY

2.1. Impact-approximation and Non-impact-approximation Theories

In the present paper, the SC impact-approximation Eqs.(56,57) [2] and the non-impact-approximation Eq.(55) [2] are used in computing $log(w) - vs - log(P)$ curve.

2.2. Unified Theory

Theoretical calculations and experimental evidence show that the electric dipole transition moment is not constant [10]. Allard *et al*. [4] derived a unified theory of spectral line shapes to take into account the dependence of the electric dipole moment upon the position of the perturbers. The details of the complete derivation are given in [4].

The important $g(s)$ term in the unified theory is given in Eq.(121)[4]. It is renumbered here as Eq.(1) and includes several minor changes: only one transition is considered and the first factor on the right of Eq.(121)[4] is taken as unity.

$$\Re[g(s)] = \int_0^\infty 2\pi\rho d\rho \int_{-\infty}^{\infty} dx \cdot \tilde{d}_{e,e'}[r(0)]\{\cos(\hbar^{-1}\int_0^s dt V_{e',e}[r(t)]) \tilde{d}_{e',e}[r(s)] - \tilde{d}_{e,e'}[r(0)]\}\ , \quad (1)$$

where $\Re[g(s)]$ has been formed from Eq.(121)[4] by using the real part of $\exp(i\hbar^{-1}...)$, namely, $\cos(\hbar^{-1}...)$. In order to put $\Re[g(s)]$ Eq.(1) into a computable form, we must first put $d_{e,e'}(\vec{r})$ Eq.(93)[4] into a computable form. We substitute the electronic basis function $\psi_{i,k}(r)$ Eq.(14)[8] for the $\chi_e(\vec{r})$ term in Eq.(93)[4] and $\psi_{f,k}(r)$ for the $\chi_{e'}(\vec{r})$ term in Eq.(93)[4]. $d_{e,e'}(\vec{r})$ Eq.(93)[4] then becomes

$$d_{e,e'}(r) = \langle \psi_{i,k}(r) \mid d \mid \psi_{f,k}(r) \rangle, \quad (2)$$

where d is generally approximated as unity. $\psi_{i,k}(r)$ was introduced in [8] as Eq.(14). Renumbered, it becomes

$$\psi_{i,k}(r) = \sum_{l=0}^{l_{max}} (2l+1) i^l \exp(i\delta_{i,l}) R_{i,l}(kr) P_l(\cos\theta), \quad (3)$$

where $\psi_{i,k}(r)$ has been expanded as a sum of partial waves. l is the angular momentum quantum number, $\delta_{i,l}$ is the phase shift, $P_l(\cos\theta)$ is the Legendre polynomial and $R_{i,l}(kr)$ is the solution to the Schroedinger equation Eq.(6)[9], renumbered below as Eq.(4), and expressed in $R_{f,l}(kr)$ terms:

$$d^2R_{f,l}/d\rho^2 + 2dR_{f,l}/\rho d\rho + [1 - 4\mu\pi V_f(\rho)c/\hbar k^2 - l(l+1)/\rho^2]R_{f,l} = 0, \quad (4)$$

where $k = \sqrt{(3\mu k_B T/\hbar^2)}$, μ is the reduced mass and only in Eq.(4), ρ =kr. Note that in Eq.(1) and in the following equations, ρ is the impact parameter.

Of the two forms, $d_{e,e'}[r(0)]$ and $d_{e',e}[r(s)]$, we choose $d_{e,e'}[r(0)]$ to derive, where $r(0) = \sqrt{(\rho^2 + x^2)}$ and x is the position of the perturber along its straight-line trajectory. For a given ρ, x and the corresponding $kr(0)$, the Schroedinger Eq.(4) is scanned through 2750 solutions until the value of the independent variable ρ matches the above value of $kr(0)$. The corresponding value of the dependent variable, $R_{f,l}[kr(0)]$, is the desired term for Eq.(5) below. Similarly, we use $V_i(\rho)$ in Eq.(4) to get $R_{i,l}[kr(0)]$ for Eq.(5).

The dipole matrix $d_{e,e'}[kr(0)]$ in Eq.(2) involves an integration over θ of the product $\psi_{i,k}[kr(0)] \cdot \psi_{f,k}[kr(0)]$ (the integration over φ equals 2π). Now from Eq.(3), this product involves a double sum, $\sum_{l=0}^{l_{max}} \cdot \sum_{l'=0}^{l'_{max}}$. In the θ integration of Eq.(2), after $\psi_{i,k}(r)$ and $\psi_{f,k}(r)$ from Eq.(3) have been entered, the orthogonality of $P_l(\cos\theta) \cdot P_{l'}(\cos\theta)$ eliminates one sum. The resulting integration over θ of the remaining sum yields

$$d_{e,e'}[kr(0)] = \sum_{l=0}^{l_{max}} (2l+1)^2 2/(2l+1) R_{i,l}[kr(0)] R_{f,l}[kr(0)]\ . \quad (5)$$

Similarly, one obtains an expression for $d_{e',e}[r(s)]$ for a given value of s, where $r(s) = \sqrt{[\rho^2 + (x+vs)^2]}$ and where the velocity $v = \sqrt{(3k_BT/\mu)}$. The integration over dt can be achieved in Eq.(1) if we set the expression for $r(t)$ equal to $\sqrt{[\rho^2 + (x+vt)^2]}$. From Eq. (117) [4],

$$\tilde{d}_{e,e'}(r) = d_{e,e'}(r) \cdot \exp[-1/2k_BT \cdot V_i(r)].$$

Thus, we have all the necessary terms for the three integrations in Eq.(1) to form $\Re[g(s)]$ for a given s. Note, $R_{i,l}[kr(0)]$ and $R_{f,l}[kr(0)]$ are implicit functions of ρ and x, and $R_{i,l}[kr(s)]$ and $R_{f,l}[kr(s)]$ are implicit functions of ρ, x and s. Similarly, we obtain $\Im[g(s)]$ by substituting $\sin(\hbar^{-1}...)$ for $\cos(\hbar^{-1}...)$ in Eq.(1). Finally, the line shapes

for different P's, can be computed from the following line-shape equation $F(\omega)$:

$$F(\omega) = 2/2\pi\int_0^{s_{max}} d\ s\exp\{-n\cdot\Re[g(s)]\}\cos\{-n\cdot\Im[g(s)]+\omega s\}. \quad (6)$$

Thus, the desired computed w's can now be obtained from measurements made on these line shapes, and these computed values of w can be put into the curves as shown in the Results Section.

3. COMPUTATIONAL DETAILS

3.1. Integration of Eq.(4)

The integration of the Schroedinger Eq.(4) to obtain $R_{i,l}[(kr(0)]$, $R_{f,l}[kr(0)]$, $R_{i,l}[kr(s)]$ and $R_{f,l}[kr(s)]$ used a second-degree Runge-Kutta method;

3.2. Expansion of Pseudo-potentials

The pseudo-potentials were expanded into 2750 elements employing a standard Spline techniqe;

3.3. Plotting of $log(w)-vs-log(P)$ curves

For a given value of P and of T, the value of w was measured from the computed line shape, $F(\omega)$ Eq.(6). The resulting w's for different P's were plotted as $log(w)-vs-log(P)$ curves. This type of a plot was used because it is linear in the case of the impact-approximation Eqs.(56,57)[2], thus allowing the slope to be easily measured and characterized;

3.4. Choice of l_{max}

The choices of l_{max} = 160 and 105 are for T=1000 and 400 K, respectively;

3.5. Choice of s_{max} at T=400 K

For the computations of $log(w)$ at T=400 K, we used the following procedure: the value of s_{max} at T=400 K is such that w at T=400 K equals w at T=1000 K+0.25 cm^{-1}. This procedure is based on the results in [8], where Fig. (**2**) [8] established that the difference between w at T=400 K and w at T=1000 K was $\approx$ 0.25 cm^{-1};

3.6. Integration of Eq.(6) over *ds*

For the integration over *ds* of Eq.(6) to obtain the line shape $F(\omega)$, a value of s_{max} was used instead of the ∞. Because of the close resemblance of the $\int dt$ factor in Eq.(121)[4] to the $\int dt'$ factor in the non-impact-approximation Eq.(55)[2], the following procedure was used: for a given P, the value of s_{max} in the unified treatment was set equal to the corresponding value of s_{max} in the non-impact-approximation treatment. The calculation of s_{max} in the non-impact-approximation treatment is described below in subsection 3.7. A grid of 100 elements was adequate to ensure convergence of the integration.

3.7. Calculation of s_{max} in the Non-impact-approximation Treatment

We summarize here the method for calculating the s_{max} values in the non-impact-approximation treatment: first, for log(P)=6, $n\cdot\Re[g(s)]$ in Eq.(6) $\approx$ 5+/-1. For simplicity, let $s_{max}[log(P)=6]$ be represented by $s_{max}(6)$. Then, $s_{max}(5)=s_{max}(6)\cdot\sqrt{(10)}$, $s_{max}(4)=s_{max}(5)\cdot\sqrt{(10)}$, $s_{max}(3)=s_{max}(4)\cdot\sqrt{(10)}$, $s_{max}(2)=s_{max}(3)\cdot 10$, $s_{max}(1)=s_{max}(2)\cdot 10$.

This procedure is based on the results of [9], where the slope of the non-impact-approximation curve is $dlog(w)/dlog(P)\approx 0.5$ and the slope of the impact-approximation curve is $dlog(w)/dlog(P)\approx$ 1.0.

4. RESULTS

4.1. Pseudo-potential Descriptions

Figs (**1** and **2**) show the pseudo-potentials, $\Delta V_1 = 7s^2S_{1/2}-4p^2P_{3/2,3/2}$, $X^2\sum_{1/2}$ - $A^2\Pi_{3/2}$ and $\Delta V_2 = 7s^2S_{1/2}-4p^2P_{3/2,1/2}$, $X^2\sum_{1/2}$ - $B^2\sum_{1/2}$, where $\Delta V = V_f - V_i$. (See [11] for a discussion of the electronic states, such as $X^2\Sigma_{1/2}-A^2\Pi_{3/2}$). In the region $R\approx 12.5$Å, the pseudo-potentials are about equal, $\approx$ -9.0, -8.3 cm^{-1}; but at $R\approx 6.3$Å, ΔV_1 has a much deeper well of -39.3 cm^{-1} as compared with the well, -8.8 cm^{-1}, in ΔV_2. The similarity in the shapes of the two pseudo-potential-differences at $R\approx 12.5$Å is attributed to the fact that both pseudo-potentials have the same final state, $7s^2S_{1/2}$; and the difference in well depths at $R\approx 6.3$Å is attributed to the difference between $4p^2P_{3/2,1/2}$ and $4p^2P_{3/2,3/2}$. The development of the pseudo-potential is best described in [2], lines 1127-1129.

4.2. Figures, Showing Pseudo-potentials, $log(w)-vs-log(P)$, $log(w)-vs-log(n)$ and $\tilde{d}_{e,e'}[r(0)]-vs-r(0)$ Curves

4.3. $w_{exptl.}$ vs $w_{compt.}$ Relations

(a) $w_{exptl.}$ values

The experimental results were reported in [6] in which measurements were made by the author on a pressure-scanned Fabry-Perot interferometer described by Kreye and

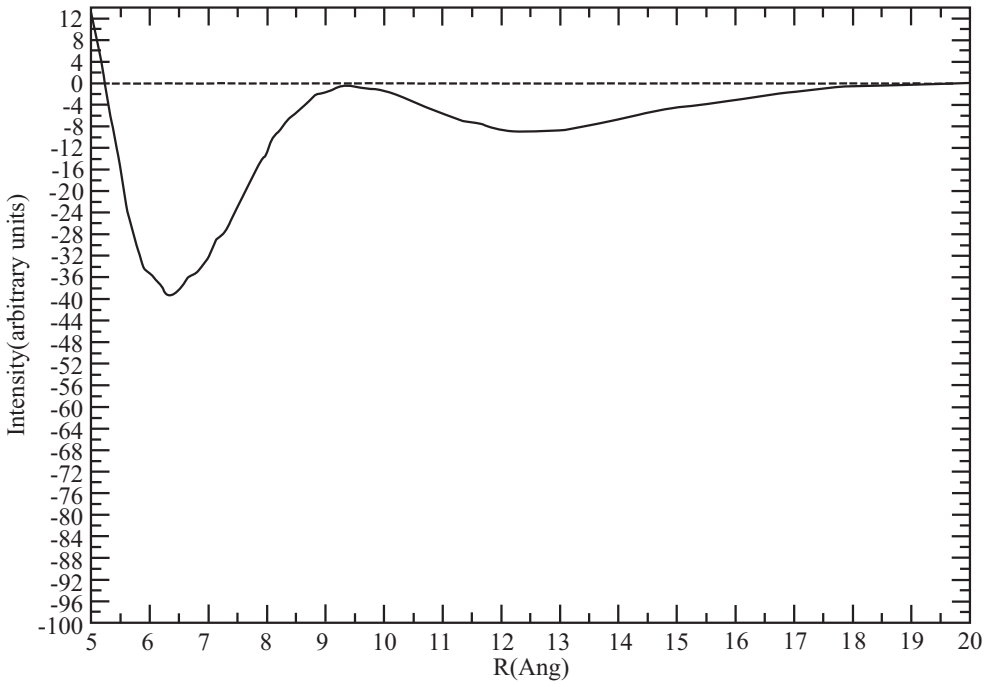

Fig. (1). This figure shows $\Delta V_1 = 7s^2S_{1/2} - 4p^2P_{3/2,3/2}$ as a function of R.

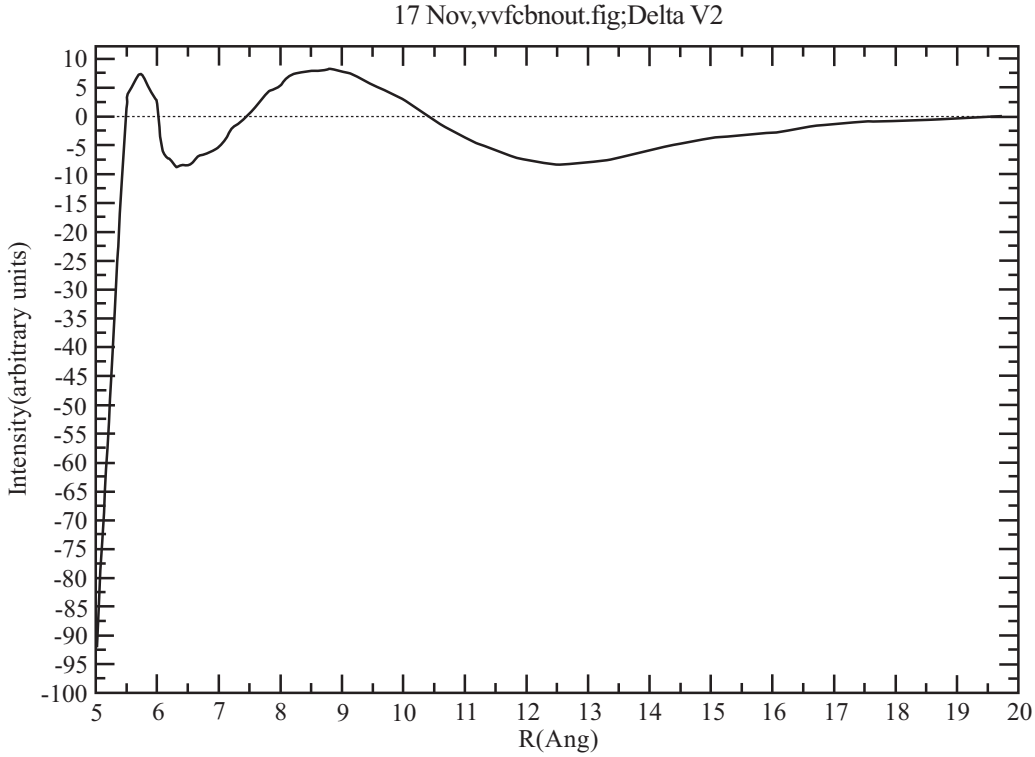

Fig. (2). This figure shows $\Delta V_2 = 7s^2S_{1/2} - 4p^2P_{3/2,1/2}$ as a function of R. Both Figs. 1 and 2 are scaled to the same vertical axis, from -100 to 12.

Roesler [12]. Fig. (**4**) [6] shows experimental values of $width/n$ in the square-symbol line as a function of T.

(a1) T=400 K

>From Fig. (**4**) [6], the value of width/n= $8.9 \cdot 10^{-20} cm^2$ at T=400 K.

At P=10 torr,

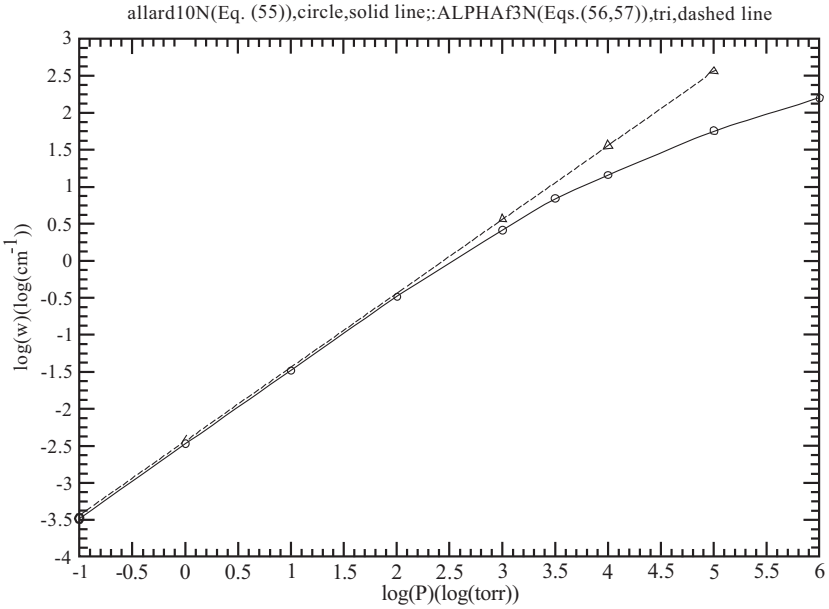

Fig. (3). This figure shows two $log(w) - vs - log(P)$ curves for the line core at T=1000 K. The solid line corresponds to the non-impact-approximation Eq.(55)[2] and the dashed line corresponds to the impact-approximation Eqs.(56,57)[2]. As expected, the impact-approximation line is linear, whereas the non-impact-approximation line approaches a constant slope at P=10^6 torr. Both curves are for ΔV_1. The smooth solid line, with no slope discontinuities, answers the question at the end of the Introduction Section, namely, can the non-impact-approximation $log(w) - vs - log(P)$ curve be plotted with no slope discontinuities?

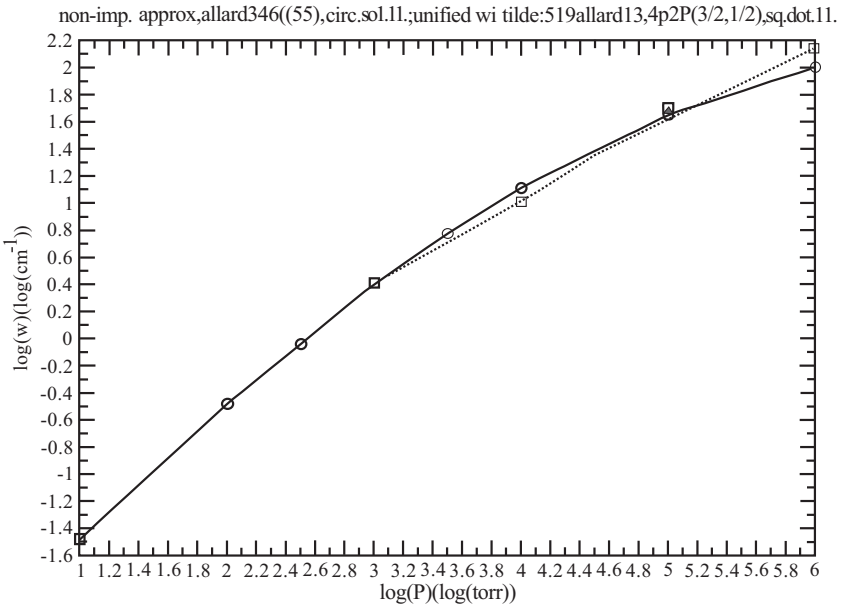

Fig. (4). This figure shows two $log(w) - vs - log(P)$ curves. The dotted line corresponds to the important unified Eq.(121)[4]. It steadily increases at P=10^6 torr. The solid line corresponds to the non-impact-approximation Eq.(55)[2], and it begins to approach a constant slope. At P=10^6 torr, the ratio of the unified-theory value of w to the non-impact-approximation-theory value is 1.12. Both lines correspond to ΔV_2 at T=1000 K.

$w_{exptl.} = 0.021\ cm^{-1}$.

(a2) T=1000 K

>From Fig. (**4**) [6], the extrapolated value of width/n= $13.4 \cdot 10^{-20} cm^2$

at T=1000 K. At P=10 torr,

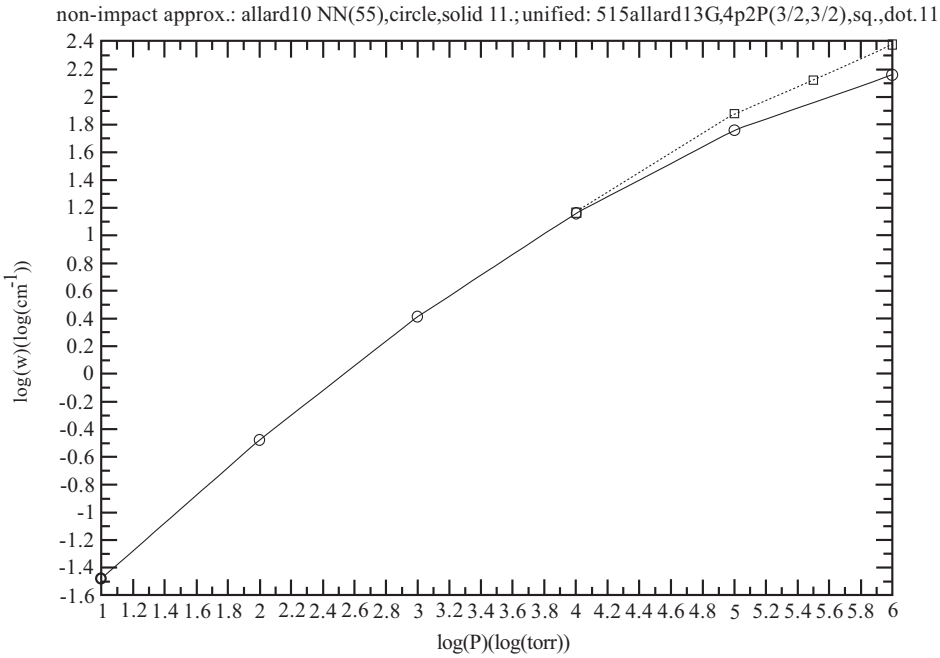

Fig. (5). This figure shows two $log(w) - vs - log(P)$ curves. The dotted line corresponds to the unified Eq.(121)[4]. The solid line corresponds to the non-impact-approximation Eq.(55)[4]. At P=10^6 torr, the ratio of the unified value of w to the non-impact-approximation value of w is 1.66. Both lines correspond to ΔV_1 at T=1000 K.

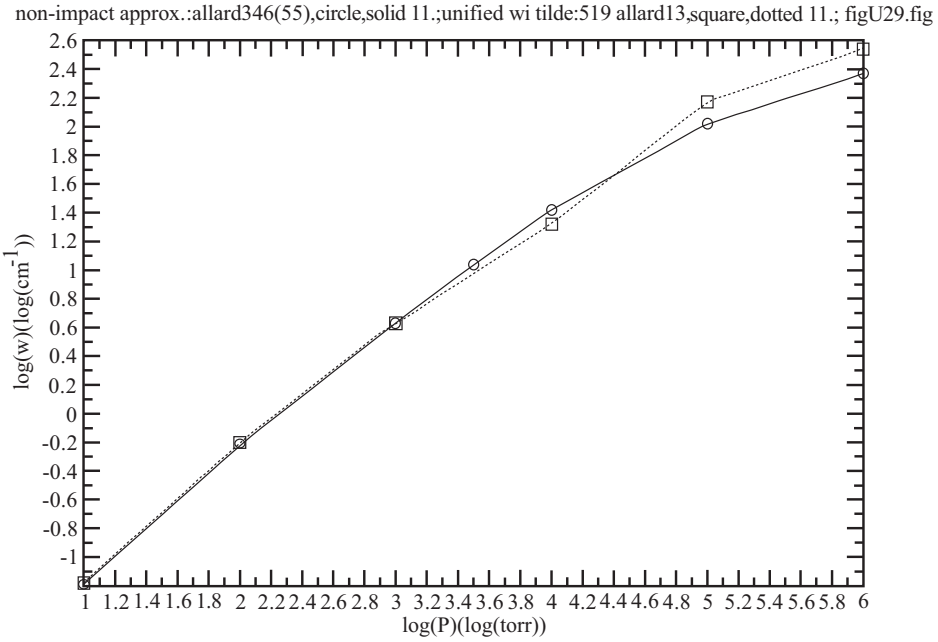

Fig. (6). This figure shows the $log(w) - vs - log(P)$ curve which is computed at T=400 K and for ΔV_2. The solid line corresponds to the non-impact-approximation Eq.(55)[2].

$w_{exptl.}$=0.013 cm^{-1}.

(b) $w_{compt.}$ values

The computed results for T=1000 K are based on analyses of spectral-line shapes for the unified theory and for the non-impact-approximation theory.

(b1) T=400 K

>From Fig. (**6**), with ΔV_2 and T=400 K, the intersection of the solid non-impact-approximation line with the horizontal axis at P=10 torr yields

$w_{compt.}$=0.0281 cm^{-1}.

(b2) T=1000 K

>From Fig. (**4**), with ΔV_2 and T=1000 K, the intersection of the dotted

unified line with the horizontal axis at P=10 torr yields

$w_{compt.}$=0.0159 cm^{-1}.

(b3) T=1000 K

>From Fig. (**5**), with ΔV_1 and T=1000 K, the intersection of the dotted unified line with the horizontal axis at P=10 torr yields

$w_{compt.}$=0.0229 cm^{-1}.

(c)Percent difference=($w_{compt.}$ - $w_{exptl.}$) 100/ $w_{exptl.}$

>From the above data at T=400 K, we compare $w_{exptl.}$=0.021 cm^{-1} with $w_{compt.}$=0.0281 cm^{-1}. The percent difference is +33%, and the average value is 0.024 cm^{-1}. At T=1000 K, we compare $w_{exptl.}$=0.013 cm^{-1} with $w_{compt.}$=0.0159 cm^{-1}. The percent difference is +22%, and the average value is 0.014 cm^{-1} .

4.4. Ratios of $w_{unif.}/w_{non-impact-approximation}$, Compared for ΔV_1 and ΔV_2

The ratio of $w_{unif.}/w_{non-impact-approximation}$ at T=1000 K, P=10^6 torr and for ΔV_1 is calculated from Fig. (**5**) in the present paper to be 1.66. The corresponding ratio for ΔV_2 is calculated from Fig. (**4**) to be 1.12. The larger ratio for ΔV_1 is attributed to its deeper well of -39.3 cm^{-1} at $R \approx 6.3$Å as compared to the corresponding well of -8.8 cm^{-1} for ΔV_2. $w_{unif.}$ is the value of w for the unified theory.

4.5. Dependence of $w_{unif.}$ upon the Depth of the Well

For this result, P=10 torr, T=1000 K. We show in the following that the $w_{unif.}$ is an increasing function of the depth of the well: for a well depth of -8.8 cm^{-1} in ΔV_2, $w_{unif.}$=135 cm^{-1}; and for a well depth of -39.3 cm^{-1} in ΔV_1, $w_{unif.}$=239 cm^{-1}.

5. CONCLUSIONS

5.1. Objective one: to Eliminate the Slope Discontinuities in the Curves in Fig. (2) [9]

The slope discontinuities in the $log(w)-vs-log(P)$ curves in Fig. (**2**) [9] are a result of using two theories: the impact-approximation theory for small log(P) and the non-impact-approximation theory for large log(P). For each theory, there is a unique linear $log(w)-vs-log(P)$ line, as demonstrated in the two intersecting straight lines for each of the three temperature-plots in Fig. (**2**) [9]. In Fig. (**3**) in the present paper, there is only one plot for T=1000 K. However, the solid-line curve exhibits no slope discontinuity; this is a result of using the non-impact-approximation theory for the whole log(P) range.

5.2. Objective Two: to Show that a Deeper Well Will Yield a Larger Value of w

In subsection 4.5, P=10 torr and T=1000 K. For ΔV_2 with a well depth of -8.8 cm^{-1}, $w_{unif.}$=135 cm^{-1}. For ΔV_1 with a well depth of -39.3 cm^{-1}, $w_{unif.}$=239 cm^{-1}. Thus, the objective is fulfilled.

5.3. Objective Three: to Compare $w_{exptl.}$ with $w_{compt.}$ and to Calculate the Percent Difference

From subsection 4.3(b2) with P=10 torr, T=1000 K and for ΔV_2, $w_{compt.}$=0.0159 cm^{-1}. From subsection 4.3(a2) with P=10 torr and T=1000 K, $w_{exptl.}$=0.013 cm^{-1}. >From subsection 4.3(c), the percent difference is $\approx 22\%$, thus fulfilling the objective.

5.4. Objective Four: to Show that the Value of w for the Unified Theory is Larger than the Value of w for the Non-impact-approximation Theory at P=10^6 Torr

From Fig. (**5**) at P=10^6 torr, T=1000 K and for ΔV_1, $w_{unif.}$ = 239. cm^{-1} and $w_{non-impact-approximation}$ = 144, cm^{-1}. Thus, the objective is fulfilled.

5.5. Objective Five: to Show that the Value of w at T=400 K is Greater then the Value of w at T=1000 K

From Fig. (**6**) at T=400 K, P=10^3 torr and for ΔV_2, $log(w_{compt.})$=0.380 $log(cm^{-1})$. From Fig. (**4**) at T=1000 K, P=10^3 torr and for ΔV_2,, $log(w_{compt.})$=0.199 $log(cm^{-1})$, thus fulfilling the objective.

6. DISCUSSIONS

6.1. QM,SC contributions to Eq.(1)

Equation (1) essentially contains an SC part and a QM part. The SC part is given by the $\int_0^s dtV_{e',e}[r(t)]$ term in Eq. (1), since it is identical, in content, with the $\int_0^s dt'V[(b^2+x^2)^{1/2}]$ term in the SC Eq.(55)[2], renumbered as Eq.(7) below (if the $\hbar^{-1}$ term is removed):

$$g(s) = 2pi\int_o^\infty bdb\int_{-\infty}^\infty dx_0[1-exp\{-i\int_0^s \hbar^{-1}V[(b^2+x^2)^{1/2}]dt'\}], \quad (7)$$

where $x = x_0 + vt'$. The QM terms of Eq.(1) are $\tilde{d}_{e,e'}[r(0)]$ and $\tilde{d}_{e',e}[r(s)]$.

6.2. Comparison of $w_{exptl.}$ with $w_{compt.}$

From Section 4.3, the percent differences between $w_{exptl.}$ and $w_{compt.}$, 33% and 22%, are admittedly large; however, the corresponding average values, 0.024 and 0.014 cm^{-1}, are measures of the absolute values of w, since the computed values of w are compared with experimental values.

In most studies, an average value is only a relative value, since it is a result of a comparison between a computed/ theoretical value and a computed/theoretical value.

6.3. Definition of $g(s)$

Broadly speaking, the $g(s)$ term contains the intricate details of the basic theory in a form which is usable in the actual spectral-line-shape expression, $F(\omega)$, which has a general Gaussian/Lorentzian form.

The $g(s)$ term is included in the $F(\omega)$ line-shape Eq.(6). One of the simplest definitions is from the impact-approximation Eq.(31) [1], $g(s) = is\langle \vec{k} \,|\, V \,|\, \psi^{+} \rangle$, where the expression $\langle\ \rangle$ represents an integration over θ, φ and r. $\vec{k}$ and ψ^{+} are defined in Eqs.(9,14) [8]. $\Re[g(s)]$ is the real part of the complex g(s).

CONFLICTS OF INTERESTS

The authors confirm that this article content has no conflicts of interest.

ACKNOWLEDGEMENTS

The author acknowledges the support of Professor John Kielkopf of the University of Louisville who made available to me his pseudo-potential programs. The author also acknowledges the support of the director and staff of CaTS at Wright State University and especially the assistance of Jeff Jones in performing the computations and the help of John Meyers and Steve Wynne in preparing the manuscript.

REFERENCES

[1] Baranger M. Simplified quantum-mechanical theory of pressure broadening. Phys Rev 1958;111: 481-93.

[2] Allard N, Kielkopf J. The effect of neutral nonresonant collisions on atomic spectral lines. Rev Mod Phys 1982; 54: 1103-82.

[3] Szudy J, Baylis WE. Profiles of line wings and rainbow satellites associated with optical and radiative collisions. Phys Rep 1986; 266: 127-227.

[4] Allard NF, Royer A, Kielkopf JF, Feautrier N. Effect of the variation of electric-dipole moment on the shape of pressure-broadened atomic spectral lines. Phys Rev A 1999; 60: 1021-33.

[5] Allard NF, Bonifaci N, Denat A. Study of the parameters of the $He(3^3S) - He(2^3P)$ line. Eur Phys J D 2011; 61: 365-72.

[6] Kreye WC, Temperature dependence of the shift, width and asymmetry of the potassium ($4p \leftarrow 7s$) 5802-Å line perturbed by argon. J Phys B At Mol Opt Phys 1982; 15: 371-86.

[7] Kreye WC. Kielkopf JF. Temperature dependence of spectral lineshifts in pressure broadening. J Phys B At Mol Opt Phys 1991; 24: 65-76.

[8] Kreye WC. Quantum-mechanical vs. semi-classical spectral-line widths and shifts from the line core in the non-impact region for the Ar-perturbed/K-radiator system. J Quant Spectrosc Radiat Transfer 2007; 107: 154-63.

[9] Kreye WC. Temperature dependences of the quantum-mechanical and semi-classical spectral-line widths and the seperation n_0 of the impact and non-impact regions for the Ar-perturbed/K-radiator system. Int J Spectrosc 2010; 2010: 1-6.

[10] Tchang-Brillet W-UL, Spielfiedel A, Feautrier N, Haner D. Collision-induced satellite for the asymptotically forbidden transition $(4^2S - 5^2S)$ of potassium perturbed by neon. J Phys B At Mol Opt Phys 1989; 22: 3915-23.

[11] Vahala LI, Julienne PS, Havey MD. Non-adiabatic theory of fine-structure branching cross sections for Na-He, Na-Ne and Ne-Ar optical collisions. Phys Rev A 1986; 34: 1856-68.

[12] Kreye WC, Roesler FL. Analysis of Hollow-Cathode-Discharge-Excited ArI,ArII and AuI Spectral-Line Profiles Measured with a Fabry-Perot Interferometer. J Opt Soc Am 1970; 60: 1100-8.

Received: July 11, 2013 Revised: August 16, 2013 Accepted: August 17, 2013